Geomechanics and Engineering, *Vol. 27, No. 3 (2021) 291-307*
https://doi.org/10.12989/gae.2021.27.3.291

Reevaluation of the design and excavation of underground oil storage cavern groups using numerical and monitoring approaches

Zexu Ning**, Maoxin Su**[a], Yiguo Xue*, Daohong Qiu[b], Zhiqiang Li and Kang Fu

Geotechnical and Structural Engineering Research Center, Shandong University, Jinan 250061, China

(Received September 21, 2020, Revised October 12, 2021, Accepted October 13, 2021)

Abstract. The bench method is widely used in the construction of underground oil storage caverns. From the perspective of single caverns, a large amount of work has been performed on the cavern stability, assuming that the influence of the auxiliary tunnels can be ignored. This paper reevaluates the necessity of auxiliary tunnels for the stability analysis. First, the equivalent continuum model is established based on a cavern group that includes auxiliary tunnels, and the space-time evolution of the displacement field after excavation in a practical sequence is studied. Then, the field monitoring time series are collected to compare the differences in deformation characteristics between the intersection and non-intersection of auxiliary tunnels and caverns. The results show that the crown settlement is significantly increased at the intersection of the caverns affected by the auxiliary tunnels. When the three-cavern group design is adopted, the stability of the middle cavern is worse, and these intersections must be reinforced. The crown settlement before excavation accounts for approximately 40%–50% of the total. As different construction stages proceed, the convergence characteristics of different feature points in a whole section are different, which is helpful for improving the understanding of the deformation space-time evolution of the excavation.

Keywords: sequential excavation method; space-time evolution; stability evaluation; field monitoring; underground oil storage caverns

1. Introduction

Underground oil storage is regarded as an effective measure to solve the energy crisis (Benardos and Kaliampakos, 2005, Goodall *et al.* 1988, Lee and Song, 2003). Underground water-sealed oil storage theory has entered a rapid stage of development in the 21st century (Benardos and Kaliampakos, 2005, Hong *et al.* 2006, Li *et al.* 2014, Li *et al.* 2020). Compared with the aboveground storage tank of the same scale, the underground water-sealed oil storage cavern has the advantages of high safety, smaller site area, low operation cost, long service life, and low pollution (Goodall *et al.* 1988, Lee and Song, 2003, Liu *et al.* 2018, Mawire, 2013, Shi *et al.* 2018, Sturk and Stille, 1995, Zhu *et al.* 2010). To meet the design requirements, higher standards are implemented for engineering geology and hydrogeology conditions; the strength of the rock mass, joint development features, hydrogeological conditions, and long-term water sealing conditions are listed as evaluation indices for the reservoir area (Ning *et al.* 2021, Xue *et al.* 2015). Geological discontinuities have a controlling influence on underground rock engineering projects in terms of strength, deformability, and permeability (Wang *et al.* 2017, Xue *et al.* 2021); in particular, they determine the water-sealing performance of underground water-sealed caverns (Aliyu *et al.* 2019, Kong and Shang, 2018, Shang *et al.* 2017, Tal *et al.* 2014). It needs to meet the two principles of water sealing and stability for the underground cavern to storage oil products (Goodall *et al.* 1988, Li *et al.* 2014, Li *et al.* 2019, Li *et al.* 2020, Ma and Zoback, 2017, Shi *et al.* 2018, Wang *et al.* 2015, Xue *et al.* 2015, Zhang *et al.* 2019). Aberg first proposed the criterion of the vertical hydraulic gradient, proposing that as long as the water pressure is greater than the gravity stress around the cavern, the storage medium would not leak (Aberg, 1977). These are the basic conditions of the water-sealed storage capability: the proportion of oil is less than that of water, the oil is insoluble in water, and it is less likely to react with water. The water pressure around the cavern is greater than the oil pressure inside the cavern, resulting in the necessary inward pressure difference (Li *et al.* 2020). The water curtain system is considered to be able to effectively provide artificial groundwater recharge and compensate for the shortfall of natural water sealing (the absence of a water curtain system causes a final water seal failure) (Wang *et al.* 2018). The layout of the water curtain hole is closely related to the joint tendency. The water curtain hole should disperse water to the furthest crack (Wang *et al.* 2015). In the functional efficiency assessment of the water curtain system using autocorrelation and cross-correlation models, it was found that the efficiency of the traditional system was low in areas with heavy rainfall (Shi *et al.* 2018). Based on these studies, Zhang *et al.* (Zhang *et al.* 2019) used field monitoring and numerical simulation to study the water-

*Corresponding author, Professor
E-mail: xieagle@sdu.edu.cn
**Joint first authorship: These authors contributed equally.
[a] Ph.D.
E-mail: sumaoxin2008@163.com
[b] Ph.D.
E-mail: qiudaohong@yahoo.com.cn

ISSN: 2005-307X (Print), 2092-6219 (Online)

sealed safety of siting a new underground water-sealed crude oil storage cavern adjacent to an existing one.

The stability of underground caverns with high sidewalls and large spans is of particular concern (Chen and Irfan, 2018, Daraei and Zare, 2018, Deng *et al.* 2015, Hoshino, 1993, Li *et al.* 2016, Lee and Song, 2003, Ma and Haimson, 2016, Mohanty and Vandergrift, 2012, Oh *et al.* 2019, Shi *et al.* 2018, Yoo, 2016, Zhuang *et al.* 2017). Zhu *et al.* proposed the evaluation criterion of rock stability, namely the ratio between the elasto-plastic displacement and the elastic displacement (Zhu *et al.* 2010). In addition, Yang *et al.* (Yang *et al.* 2014) studied the anisotropic properties of fractured rock masses, accounting for the coupled effect of seepage and stress. The stress path of the rock mass during excavation determines the disturbance of the surrounding rock mass to a large extent, which is reflected in the convergence degree and the plastic zone range (Ma and Haimson, 2016). A boundary element code (LaModel) was used to develop numerical models with weakened peripheral elements to account for the possible deterioration of cavern pillars, and the long-term stability of an underground propane gas storage cavern in the sedimentary rock formations was analyzed, indicating that its service life can be extended for 30 years (Mohanty and Vandergrift, 2012). Using discontinuous deformation analysis (DDA), He and Zhang numerically studied the formation of the pressure arch and the stabilization mechanism of rock bolts for underground excavation in laminated rock mass, determining the influences of in situ stress ratio, joint friction angle, overburden depth, and dip angle on the pressure arch (He and Zhang, 2015). A conceptual hydrogeological model for assessing the containment properties of underground water-sealed oil storage caverns was developed for evaluating the containment properties of underground caverns (Qiao *et al.* 2016). Crack slip is unfavorable to the stability of the surrounding rock. The continuous-discontinuous element method (CDEM) and six-channel mass spectrometry (MS) monitoring systems were used to capture micro-cracks, which helps to understand the mechanism of rock mass deformation at the microscopic scale (Hong *et al.* 2006, Ma and Haimson, 2016, Ma and Zoback, 2017). Based on cloud theory and the principal component analysis (PCA) method, Li *et al.* proposed a novel analytical model for the surrounding rock classification (SRC) of underground water-sealed caverns, and they calculated a multi-index certainty degree combined with the weights as guidance in classifying the surrounding rock (Li *et al.* 2019). However, the previous studies on the excavation stability of underground tunnel were mostly based on the excavation results and disregarded the excavation process itself and the changes before excavation. The excavation process of a large cavern is complex and the time of a cyclical footage is relatively long; therefore, the distribution law of different construction steps must be studied along with the section positions in the excavation process. This study was aimed at filling up this research gap and analyzing the space–time evolution of displacement field before and after the excavation.

Due to the uncertainty of the geological structure and rock mass properties, as well as the large number of underground facilities and complex spatial distribution, there is still no unified understanding of the overall stability mechanism of underground reservoirs. In underground facilities, auxiliary tunnels have a small span and cross section, and the influence of the auxiliary tunnel on stability is relatively weak compared to that of the storage cavern, which has rarely been mentioned in previous studies. Therefore, as a novel perspective, we consider the smallest underground engineering facilities unit, a cavern group, which includes auxiliary tunnels (construction tunnels and connection tunnels). In this paper, a rethinking of the stability of underground water-sealed oil storage caverns in the design of a cavern group is detailed, and the corresponding steps of sequential excavation are explained. In this study, we determined some of the advantages and disadvantages of the design aspect of the cavern group and analyzed the relationship between the total and crown displacements after the excavation. A comprehensive analysis method based on finite element calculation and field monitoring is proposed, providing guidance for engineering design and stability maintenance.

2. Area description

2.1 Project profile

This study is based on the Huangdao underground water-sealed oil storage cavern, which is located in eastern China. The storage cavern is oriented in a northwest direction, 600 m wide from east to west, and 838 m long from north to south. The designed underground engineering (see Fig. 1) mainly includes six construction tunnels and 10 connecting tunnels (yellow), nine storage caverns (black), six vertical wells, and five water curtain tunnels (blue). The designed storage capacity is 300 × 104 m^3. According to structural characteristics, the construction tunnel is supported by systematic bolts and fiber reinforced shotcrete. The design size is shown in Fig. 1, and the design section is a straight wall and circular arch (see Fig. 2). The designed length of the connection tunnel is 109 m and the longitudinal slope is 0%. The bottom surface elevation of the storage cavern is -50 m, with a span of 20 m and a height of 30 m. The distance between the cavern wall and the adjacent construction tunnel wall is 25 m. Each of the three caverns is connected by a connection tunnel to form a cavern group, which is divided into three cavern groups. A planar and section graph of the reservoir area is shown in Fig. 3.

The formation lithology around the storage area mainly is comprised of granitic gneiss, deluvium, alluvial-pluvial deposits, lamprophyre, and diorite veins. The reservoir area can be divided into five areas (labeled I-V) according to the strike of the geologic discontinuities. The joint direction of area I is mainly NW 345°. Area II is the transition zone, and its joint direction is mostly in the north-south direction. Area III has a nearly north-south direction, with discontinuities in the NE 45° direction. Area IV has discontinuities mainly in the NE 45-60°, NE 30 °, and

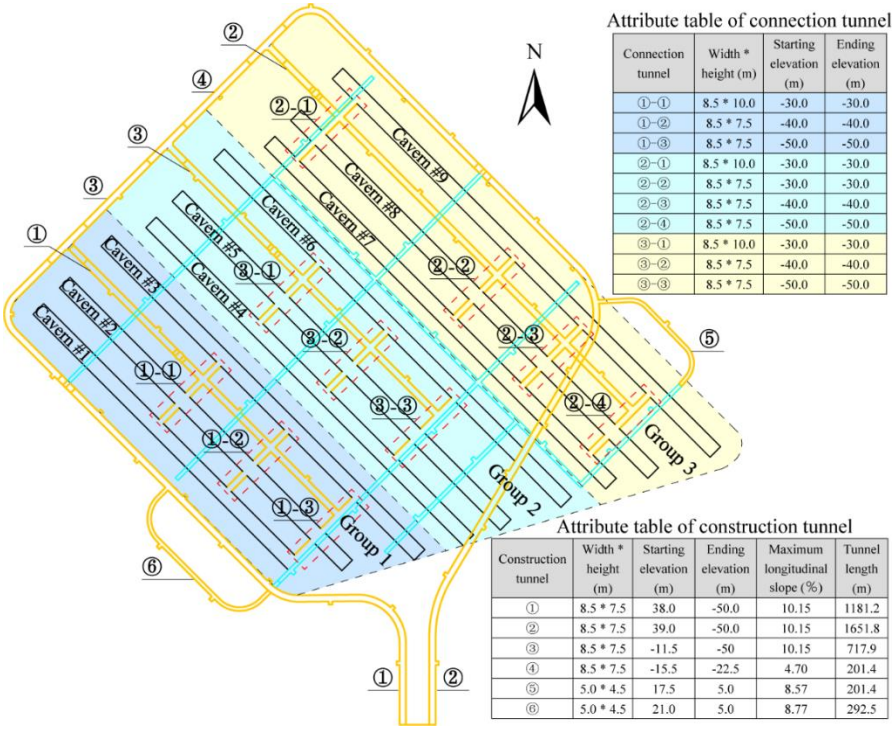

Attribute table of connection tunnel

Connection tunnel	Width * height (m)	Starting elevation (m)	Ending elevation (m)
①-①	8.5 * 10.0	-30.0	-30.0
①-②	8.5 * 7.5	-40.0	-40.0
①-③	8.5 * 7.5	-50.0	-50.0
②-①	8.5 * 10.0	-30.0	-30.0
②-②	8.5 * 7.5	-30.0	-30.0
②-③	8.5 * 7.5	-40.0	-40.0
②-④	8.5 * 7.5	-50.0	-50.0
③-①	8.5 * 10.0	-30.0	-30.0
③-②	8.5 * 7.5	-40.0	-40.0
③-③	8.5 * 7.5	-50.0	-50.0

Attribute table of construction tunnel

Construction tunnel	Width * height (m)	Starting elevation (m)	Ending elevation (m)	Maximum longitudinal slope (%)	Tunnel length (m)
①	8.5 * 7.5	38.0	-50.0	10.15	1181.2
②	8.5 * 7.5	39.0	-50.0	10.15	1651.8
③	8.5 * 7.5	-11.5	-50	10.15	717.9
④	8.5 * 7.5	-15.5	-22.5	4.70	201.4
⑤	5.0 * 4.5	17.5	5.0	8.57	201.4
⑥	5.0 * 4.5	21.0	5.0	8.77	292.5

Fig. 1 Layout of auxiliary tunnels and main caverns

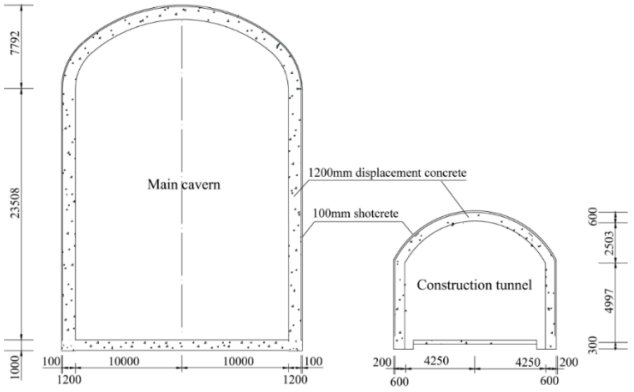

Fig. 2 Cross sections of storage cavern and construction tunnel

nearly north–south directions. The discontinuities of area V are mainly in the NW 330-345 ° and less northeast directions. There are mainly two fault zones: in the northeast strike and near the west-east strike. The fold structure is not developed. The fault only has influence on the site selection of the reservoir area, but not on the construction. The rock mass is classified according to the "Standard for engineering classification of rock mass" (GB/T50218-2014), which indicates that the proportion of surrounding class II and III rocks in the reservoir area is the largest, and that the whole rock mass has good stability.

The physical and mechanical indices of the rock mass were obtained by field and laboratory tests. The permeability coefficient of the surrounding rock was obtained through a cross-borehole interconnectivity test, curtain system injection test, and water pressure test (Wang *et al.* 2015). Parameters such as the elastic modulus, Poisson's ratio, and compressive strength of the geologic discontinuity of the rock were obtained by uniaxial and triaxial tests and shear-percolation coupling tests (see Table 1). The space distribution of deviator stress-average principal stress was obtained by triaxial compression test, determining the shear contractive and dilatancy zones.

2.2 Construction method

Smooth or pre-splitting blasting was used in the excavation of the auxiliary tunnels and storage caverns. The rock mass in auxiliary tunnels was mostly class II and III. The geological condition was good and the section size was small, and thus the full-face excavation method was used. In contrast, the sidewall of the storage cavern was high and the span was large. To ensure stability during construction, the sequential excavation method was adopted. The excavation of the cavern arch played a guiding role in the entire excavation process, and reasonable subsequent excavation and support schemes were selected according to the actual disclosed geological conditions. Therefore, the excavation of the lower steps after the excavation of the upper step was safer. According to the geological conditions, the middle drift (height: 8.5 m, span: 12 m, cyclical footage: 2.5-3.5 m) could be excavated first. The advance prediction and advance water exploration carried out in the middle guide hole can effectively reduce the loss of groundwater during construction. After the completion of a middle drift, we expanded the construction on both sides (by 4 m) via smooth blasting. After the completion of the first step, the second and third steps were excavated via pre-splitting blasting excavation on both sides (height: 9.5 m, span: 20 m, and cyclical footage: 9.5 m), and the bottom protective layer was excavated via smooth blasting excavation (height: 2.5 m, span: 20 m, and cyclical footage: 9.5 m).

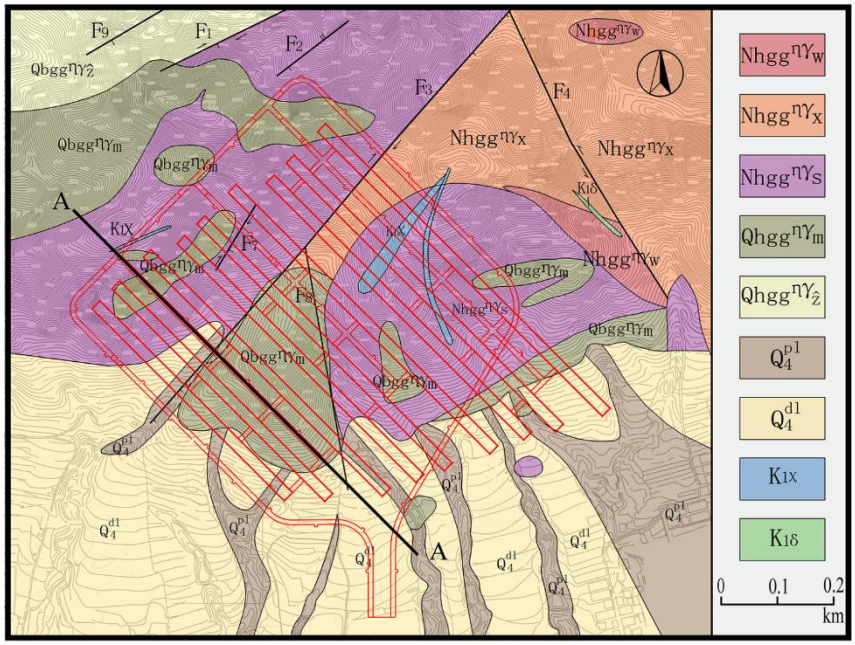

(a) The geology map of the reservoir area

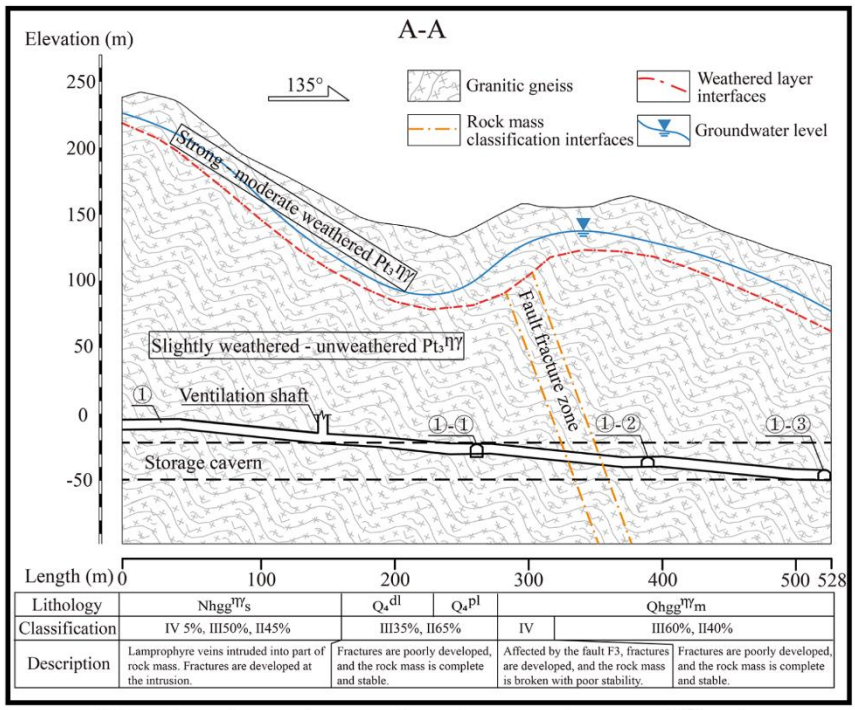

(b) Engineering geology section of construction tunnel ① axis

Fig. 3 Geological map of the reservoir area: (a) planar graph and (b) section graph

Table 1 Physical and mechanical parameters of rocks in the reservoir area

Description	Mass density (g/cm^3)	Saturated UCS (MPa)	K	E (GPa)	Poisson ' s ratio	SSI		T (MPa)	ERC (MN/m^3)
						Cohesion (MPa)	IFA (°)		
S1	2.64	86.99	0.77	48.3	0.18	8.14	58.79	12.24	4093
S2	2.59	60.89	0.67	38.3	0.17	7.0	47.59	6	3273
S3	2.81	72.82	0.89	64.6	0.26	5.32	66.32	11.76	5127

*S1: Slightly weathered porphyritic fine granitic gneiss; S2: Moderate weathered porphyritic fine granitic gneiss; S3: Lamprophyre veins; UCS: uniaxial compressive strength; ERC: elastic resistance coefficient; E: Elastic Modulus; T: Tensile strength; K: Softening coefficient; SSI: Shear strength indices; IFA: Internal friction angle

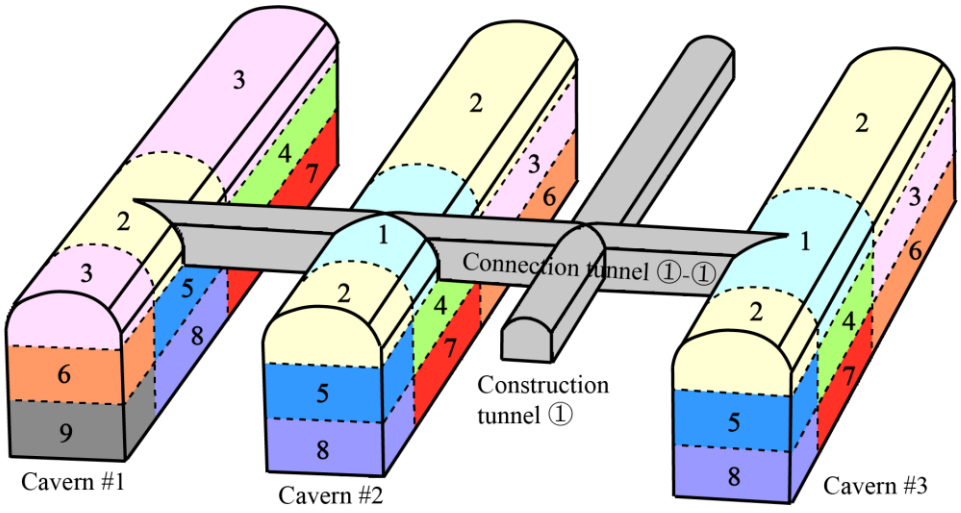

Fig. 4 Excavation sequence of intersection between storage caverns and connection tunnel

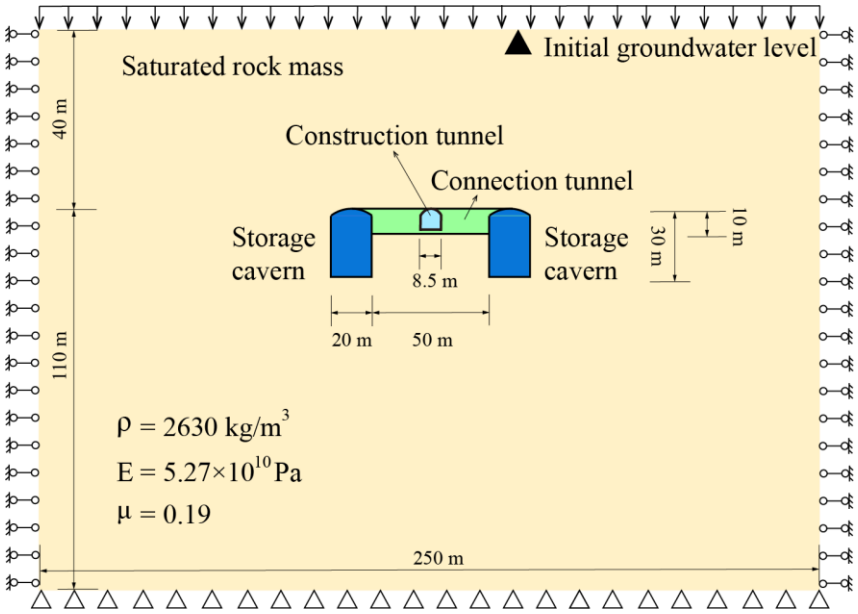

Fig. 5 Geometric and boundary conditions of the design-A modeling

The excavation of the auxiliary tunnel preceded that of the storage cavern, and after the excavation and support of the construction tunnel was completed, the connection tunnel was excavated. Taking cavern group 1 as an example, the intersecting characteristics and excavation sequence of the intersection are shown in Fig. 4. The main cavern was excavated in mainly three steps from top to bottom. The overall excavation sequence is marked in Fig. 4 with Arabic numbers, and the actual length of each step is determined according to the actual geological conditions. After the excavation steps 1-9 were completed in sequence, the traditional three-step excavation method was used to continue the excavation in opposite directions (NW and SE) in the cavern until the design mileage was reached.

Special attention should be paid to the protection of the groundwater level in the construction stage. Fractures distributed in rock mass and sidewalls are important channels for groundwater inflow. In the construction process, the disturbance to the surrounding rock should be reduced as much as possible, and pre-reinforcement can be carried out before excavation if necessary. For the faults and the developed dike, the surrounding rocks should be reinforced by backfilling concrete replacement after excavation. In order to maintain the minimum water head (minimum of 20 m above the water curtain holes) when the construction tunnel is at an elevation of 30 m, shotcrete or grouting should be used to treat the seepage position according to the requirements of the code.

3. Design and stability assessment

3.1 Numerical modeling

Numerical simulation has advantages in the design and evaluation of large-scale engineering projects (Nawel and

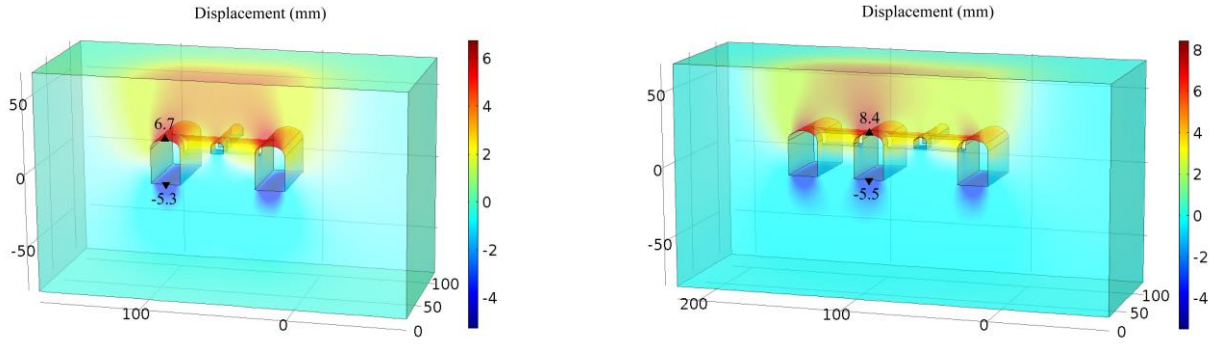

(a) design-A (b) design-B

Fig. 6 Distribution of displacement field after excavation

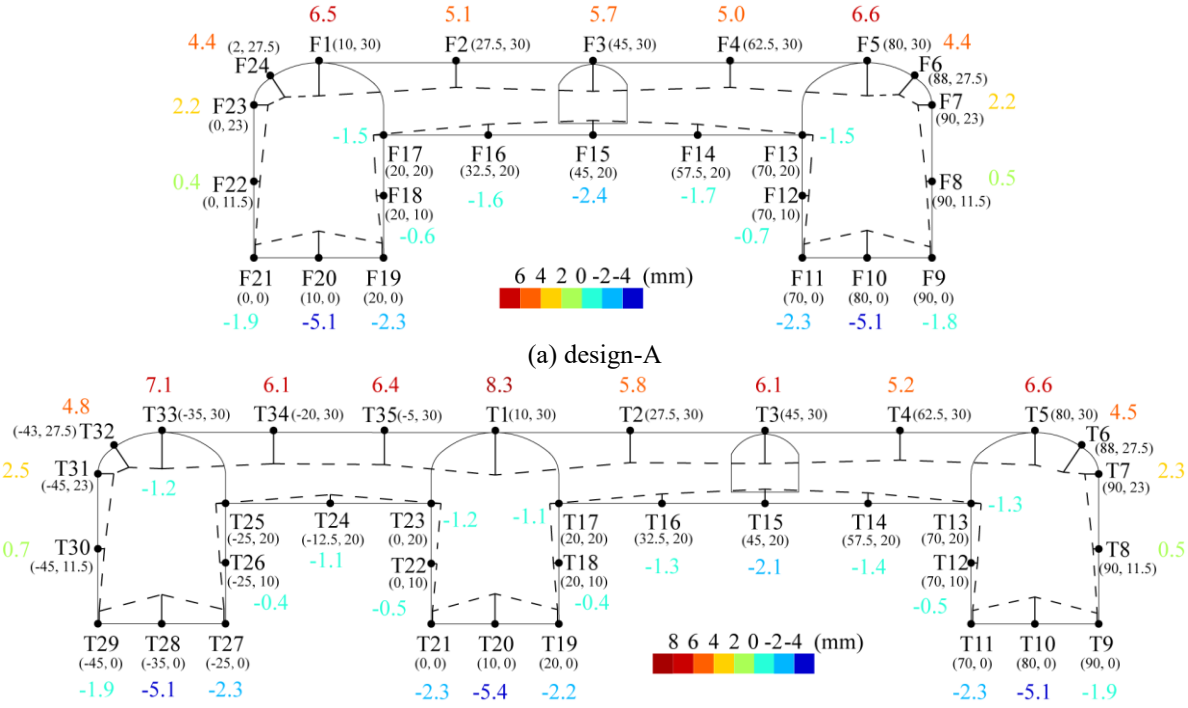

(a) design-A

(b) design-B

Fig. 7 Tangential displacement of feature points after excavation

Salah, 2015). It is not necessary to rely on the actual site data, as the numerical calculation can test and compare the proposed construction scheme and guide the engineering. We used the finite element analysis simulation software COMSOL to study the design and excavation aspects of a cavern group, and proposed a possible optimization plan. The model adopted the same cross-section size, shape, design depth, and geological conditions of the underground oil storage caverns of the Huangdao project. The 3-D distribution characteristics of the displacement field at the intersection of the auxiliary tunnels and storage caverns were studied. For stability enhancement, we propose a potential optimized design of the cavern group, which is composed of two caverns, one construction tunnel, and three or four connection tunnels (designated as design-A). As mentioned above, the underground part of the Huangdao project consists of three cavern groups, and an underground cavern group is composed of three caverns, one construction tunnel, and three or four connection tunnels (designated as design-B). The characteristics and feasibility of the displacement field of these two designs were analyzed.

Fig. 5 is a 2-D schematic diagram of the proposed design-A. All models used in the calculation were 3-D models. The following hypotheses were made for the rock mass in the models:

1) The rock mass is an equivalent continuous medium, homogeneous, and isotropic.
2) The elastic-plastic mechanical model is used for the deformation of the rock mass.
3) After the excavation of the tunnel, the deformation of the rock mass satisfies the Mohr-Coulomb criterion.
4) The initial stress of the rock mass only considers the influence of gravity stress and does not consider the tectonic stress.

The solid phase boundary conditions were as follows. The upper boundary was the stress boundary, which is equivalent to the gravity of the upper rock mass. The lower boundary was a fixed constraint boundary that limits the displacement. The four side boundaries were provided with roller supports, the displacement vertical to the boundary surface was 0, and the direction parallel to the boundary surface was free to move. The tunnel face, sidewalls, and side boundaries of the model were all free surfaces and did not restrict the displacement.

3.2 Design of a cavern group

The displacement characteristics after the excavation of design-A and design-B were compared, with an emphasis on the maximum displacement point of the surrounding rock. Because the quality of the surrounding rock is good, the plastic deformation of the cavern excavation is not concerned in the analysis, and the plastic strain zone is not significant. The 3-D model had a height of 150 m and a length of 100 m. The model width was determined by the number of caverns. The model of design-A was 250 m, and that of design-B was 295 m. Both sides of the cavern were widened by four times the span (80 m) to the side boundaries of the model. The calculation results are shown in Figs. 6 and 7. In order to highlight the differences between the two designs, we counted the changes in some feature values in Table 2.

Table 2 Tangential displacement contrast of feature points

Feature point, F	Displacement (mm)	Feature point, T	Displacement (mm)	Displacement difference, T − F (mm)	Trend
F1	6.51	T1	8.31	1.80	Rising
F2	5.08	T2	5.79	0.71	Rising
F3	5.69	T3	6.10	0.41	Rising
F4	5.01	T4	5.25	0.24	Rising
F5	6.57	T5	6.64	0.07	Rising
F9	-1.84	T9	-1.86	-0.02	Rising
F10	-5.14	T10	-5.06	0.08	Falling
F11	-2.29	T11	-2.25	0.04	Falling
F12	-0.67	T12	-0.45	0.22	Falling
F13	-1.48	T13	-1.28	0.20	Falling
F14	-1.67	T14	-1.43	0.24	Falling
F15	-2.42	T15	-2.14	0.28	Falling
F16	-1.63	T16	-1.26	0.37	Falling
F17	-1.47	T17	-1.10	0.37	Falling
F18	-0.62	T18	-0.35	0.27	Falling
F19	-2.33	T19	-2.22	0.11	Falling
F20	-5.12	T20	-5.38	-0.26	Rising
F21	-1.93	T21	-2.32	-0.39	Rising

Note: Positive and negative values indicate downward and upward displacements, respectively. The trend represents the displacement change of feature point after changing from cavern group design-A to cavern group design-B.

After the excavation was completed, the crown arch settled and the bottom floated at the intersection of the main caverns and auxiliary tunnels, which was consistent with the field monitoring results.

1) In Fig. 6(a) and Fig. 7(a), the maximum crown settlement of the main caverns was 6.7 mm, and the maximum crown settlement of the connection tunnel was 5.7 mm, both occurring at the intersection. The maximum bottom floating of the main cavern was -5.3 mm, and the maximum bottom floating of the connection tunnel was -2.4 mm, which was located at the bottom midpoint of the intersection.

2) In Fig. 6(b) and Fig. 7(b), the crown settlement of the middle cavern, which was 8.3 mm, was the largest among the four intersections. The maximum crown settlement of the west cavern (far from the construction tunnel) was 7.1 mm, and that of the east cavern (close to the construction tunnel) was 6.6 mm. The crown settlement of the construction tunnel was 6.1 mm. The maximum bottom floating of the middle cavern was -5.5 mm.

3) Combined with Table 2, the displacement characteristics of the two designs were compared. For the cavern group of design-A, if we plan to add a cavern by extending the length of the connection tunnel, some changes will occur: the crown settlement of the middle cavern will increase by 1.80 mm (T1), which is the most obvious. Other feature points that will change significantly in displacement include T2-T4, T9, T20, and T21. This indicates that an additional cavern will result in the most obvious settlement increase at the crown arch of the connection tunnel between the middle cavern and the construction tunnel. In addition, the displacement of the T10-T19 feature points decreased, indicating that the displacement of design-A was lower at the bottom of the caverns and connection tunnel.

4) The displacement of the west additional cavern (far from the construction tunnel) was between the middle cavern and the east cavern. Compared with the connection tunnel in the east, the crown settlement of the connection tunnel in the west was larger, while the bottom floating was smaller.

Therefore, after the adjustment from design-A to design-B, the stability of the middle main cavern was most seriously affected. Thus, it was necessary to focus on monitoring and strengthening the support of the middle cavern. If the uncertainty of the engineering geology can be accounted for and the stability of the surrounding rock can be guaranteed, then design-B has higher feasibility and efficiency.

3.3 Space-time evolution of the displacement

According to the construction sequence, the displacement field in each construction step was simulated (Yoo and Choi, 2018). The space-time evolution law after the excavation of the whole cavern group is now discussed. The excavation sequence was consistent with reality, which is a three-step method: the middle and east caverns were excavated synchronously, and the west cavern was excavated one step later (see Fig. 4). The tangential displacement of the cross section was studied.

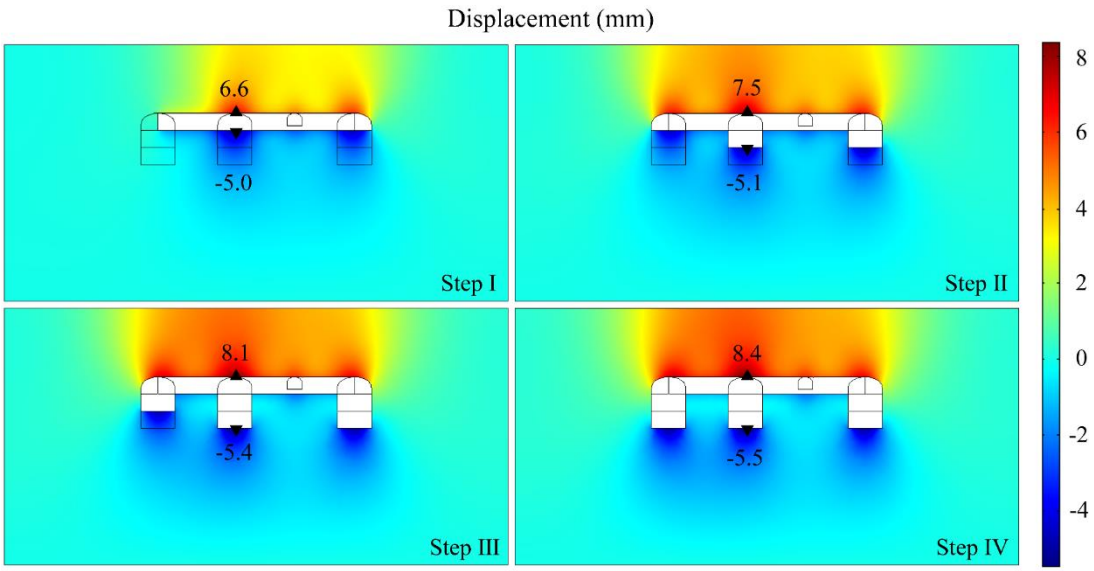

Fig. 8 Space-time evolution of displacement field after sequential excavation of the cavern group: Step I-Step IV

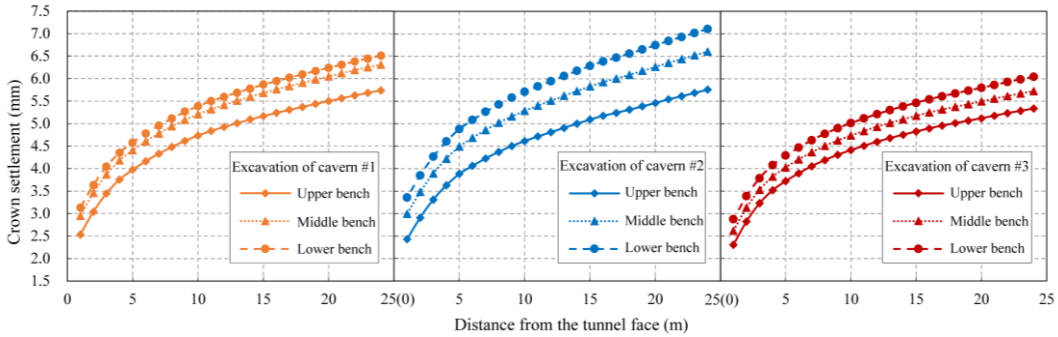

Fig. 9 Crown settlement behind the tunnel face for three-bench excavation method: cavern #1, #2, and #3

Table 3 Space–time evolution of the tangential displacement for feature points after excavation

Location	Feature points	Description	Notes
Arch of caverns and connection tunnel	T1-T7, T9, T11, T21, T34, T35	The convergence increases continuously, and the maximum is in step I.	-
Middle point at the bottom of caverns	T10, T20	The convergence of steps I-III is basically the same, and step IV is basically zero.	-
The sidewalls of caverns and the bottom of connection tunnel	T8, T12-T19, T22-T24, T30	Strong convergence in step I, weak convergence and strong settlement in steps II-IV.	Due to the excavation of the middle and lower steps, overall settlement occurs, which leads to the decrease of the convergence value at the bottom of the connection tunnel.
Inside wall of caverns	T25	Strong convergence in steps I and II, and weak convergence in steps III and IV.	Under the action of lateral and gravity stress, vertical settlement and horizontal convergence occur simultaneously at the sidewalls after the excavation of the lower steps, and the regularity is weak.
	T26	Strong convergence in steps I-III and weak convergence in step IV.	
Bottom and spandrel of caverns	T27-T29, T31	The convergence of step I is basically zero and steps II-IV are basically the same.	-
Arch of caverns	T32, T33	The convergence increases continuously, and the maximum is in step II.	-

When using the sequential excavation method to construct the intersection of the cavern group, the crown settlement and the bottom floating of the middle cavern in the whole area were the maximum (see Fig. 8). In Fig. 9, according to different caverns, the crown settlement in the range of 0-25 m behind the tunnel face during excavation was distinguished. The curve in Fig. 9 does not tend to be stable eventually, which indicates that the construction

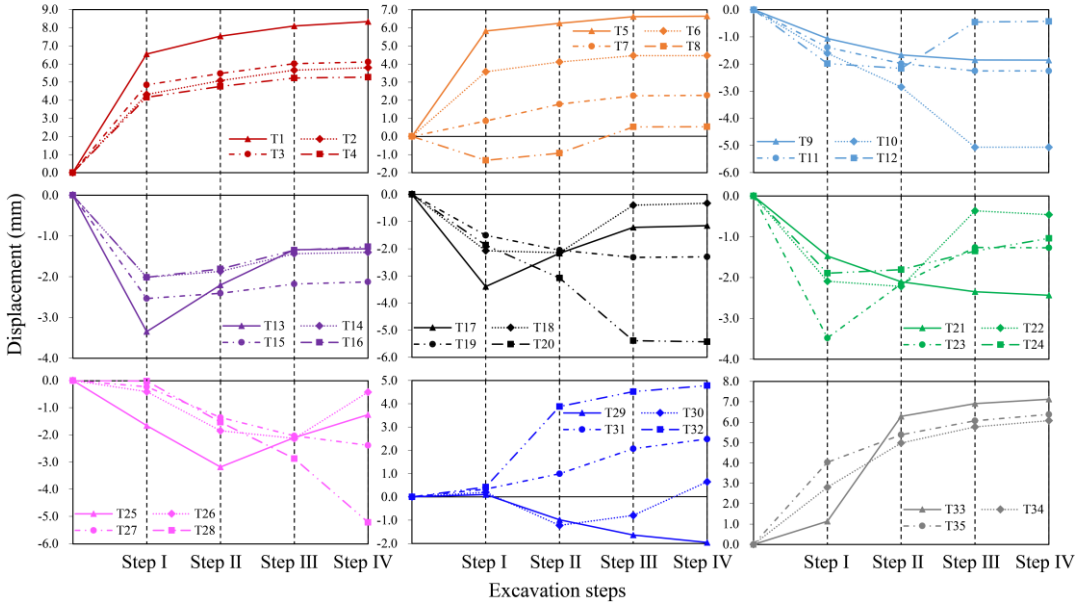

Fig. 10 Space-time relation between excavation steps and tangential displacement

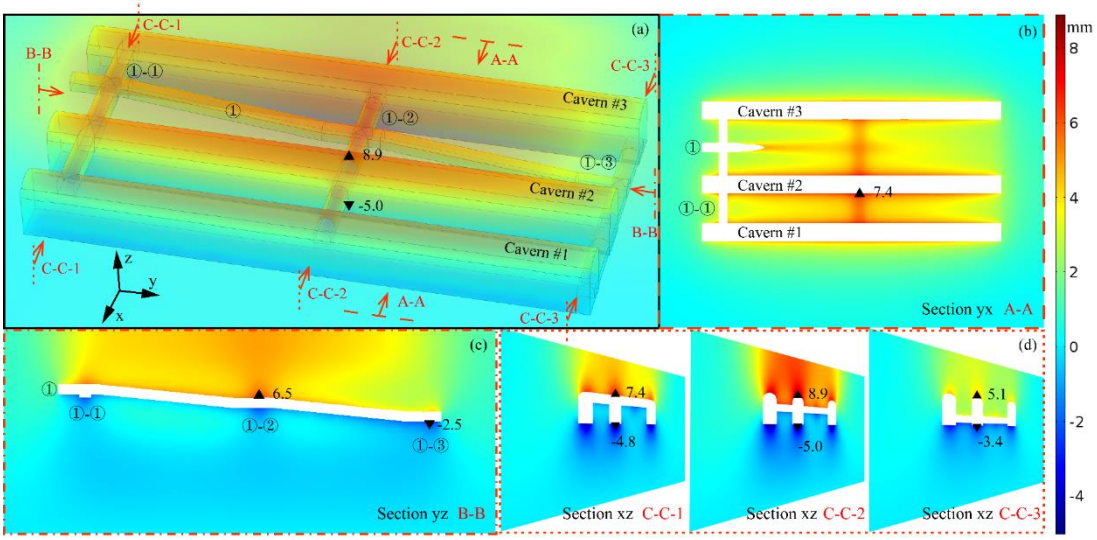

Fig. 11 The distribution characteristics of the final displacement in the excavated cavern group area: 3-D cloud map and 2-D section map

behavior of the tunnel face has a non-negligible impact on the stability of surrounding rock, within 25 m behind. The position where the crown settlement is basically stable (not significantly disturbed by construction) should be is greater than 25 m away from the tunnel face. It also shows that the deformation of surrounding rock of the large-span cavern excavation has significant time-space effect. The settlement value in the range of 5 m behind the face changed rapidly, which indicates the importance of timely support. In Fig. 10, with the different excavation steps, the displacement characteristics of different points in the section were different. In particular, the displacement growth rate of the arch continued to decrease, indicating that the excavation of the upper step had a greater disturbance to the arch than that of the lower step. In Table 3, the feature points with the same law are summarized, and the displacement evolution of various feature points is analyzed in detail.

The regional model of cavern group 1 was established with a size of 295 m × 190 m × 363 m (see Fig. 11). The storage caverns with a length of 300 m were selected for the study, including three connection tunnels and one construction tunnel. Five slices were selected to highlight the displacement of corresponding regions, which are marked in Fig. 11(a). The elevation of the three connection tunnels decreased by 10 m from west to east. In the region, the displacement of the surrounding rock at the intersection of main cavern #2 and connection tunnel ①-② was the largest. It was also found that:

1) Section A-A in Fig. 11(b) was the horizontal slice of the spandrel of connection tunnel ①-①. The spandrel settlement was 7.4 mm at the intersection of main cavern #2 and connection tunnel ①-②. Therefore, in this region, the arch settlement was the maximum.

(a) initial segment of construction tunnel ①

(b) interior view

(c) settlement measurement using a total station

(d) convergence measurement using a convergence meter

Fig. 12 Excavation and field monitoring of auxiliary tunnel

2) Section B-B in Fig. 11(c) was a radial slice of construction tunnel ①, revealing the overall stability of the upper surrounding rock at the intersection of the construction tunnel and connection tunnels. The crown settlement was the largest at position C-C-2, and the bottom floating was the largest at position C-C-3.

3) Section C-C in Fig. 11(d) was a tangential slice of three intersections. Among the three caverns, the surrounding rock stability of the middle cavern was the worst. Among the three intersections, the settlement of section C-C-2 was the largest, while that of section C-C-3 was the smallest. The stability of the connection tunnel was good.

4. In situ monitoring of excavation

4.1 Monitoring plan

For a large project, field data monitoring and analyses are valuable in assessing the variation rules and understanding the functional mechanism of the project (Ma *et al.* 2016, Shi *et al.* 2018). In order to meet the requirements of engineering design for cavern stability and verify the practical effect of design-B, it was necessary to select the monitoring items that can reflect the overall stability of caverns. The monitoring project should be able to reflect the surrounding rock deformation and supporting force. Compared with other industries, underground water-sealed oil storage caverns are complex: they have no lining and are high density. Thus, it is necessary to meet the requirements of not only the stability monitoring, but also the integrity monitoring of the cavern group.

After the excavation of the underground tunnel, the convergence deformation of the rock mass around the tunnel and crown settlement are the most direct physical quantities that reflect the rock mass deformation and the supporting force. In order to study the displacement characteristics of the cavern group, the crown settlement and surrounding rock convergence of the construction tunnel (see Fig. 12) and connection tunnel were monitored. The convergence deformation of the surrounding rock was monitored by a digital steel rule convergence meter with a minimum reading of 0.01 mm. The crown settlement was monitored by a total station with a nominal accuracy of ±1 mm.

4.2 Stability characteristics of the excavation

4.2.1 Construction tunnel

The monitoring data of the crown settlement and surrounding rock convergence of the construction tunnel were compared. The crown settlement measuring points were arranged at the middle point of the crown arch. The measuring points of the surrounding rock convergence were used as the measuring points of the crown settlement. Before measurement, we needed to lay out the base points

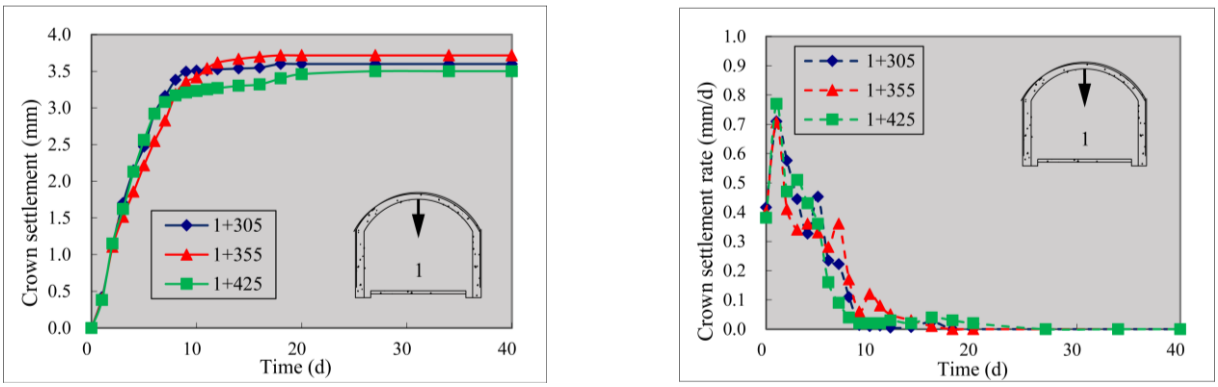

(a) crown settlement of construction tunnel ①

(b) crown settlement rate of construction tunnel ①

(c) crown settlement of construction tunnel ②

(d) crown settlement rate of construction tunnel ②

Fig. 13 Crown settlement curve of construction tunnel after excavation

Table 4 Crown settlement analysis of each monitoring section in construction tunnels

MS	MT (d)	MaxS (mm)	RDV (%)	T_1 (d)	MSR (mm/d)	T_2 (d)	OSR (mm/d)	TSC
1+305, ①	40	3.60	0.045	18	0.71	2	0.09	Stable
1+355, ①	40	3.72	0.047	16	0.71	2	0.09	Stable
1+425, ①	40	3.50	0.047	20	0.77	2	0.09	Stable
1+495, ②	40	3.60	0.045	18	0.66	2	0.09	Stable
1+570, ②	40	3.32	0.042	38	0.64	2	0.08	Stable
1+630, ②	40	3.40	0.043	40	0.56	1	0.09	Stable

*MS: Monitoring section; MT: Monitoring time; MaxS: Maximum settlement; RDV: Relative displacement value; T1: Time taken to reach maximum settlement; MSR: Maximum settlement rate; T2: Time between maximum settlement rate and start of monitoring; OSR: Overall settlement rate; TSC: Trend of settlement curve

and measure their elevation. During the measurement, the height difference between the base point and the settlement point can be measured by the total station to obtain the elevation of the measuring point. The difference between the two elevations before and after the measurement is the crown settlement of the measuring point.

Crown settlements in 1+305, 1+355, and 1+425 of construction tunnel ① and those in 1+495, 1+570, and 1+630 of construction tunnel ② are shown in Fig. 13. Table 4 compares the crown settlement data of each measuring point in the construction tunnel. According to the results, under the current surrounding rock and supporting conditions, the crown settlement characteristics of the construction tunnel are as follows:

1) Crown settlement will occur after the excavation of the construction tunnel; therefore, it is very important to implement reasonable support and reinforcement measures to control the crown settlement.

2) The maximum crown settlement is 3-4 mm, and the ratio of crown settlement to tunnel diameter is less than 0.05%. According to the control standard of displacement relative values, the allowable relative displacement should not exceed 0.5% for the current condition of buried depth and surrounding rock grade; therefore, it meets the requirements. When the settlement is more than 4 mm, attention should be paid to strengthening the support to control the settlement.

3) In general, the settlement tends to be stable at 10-

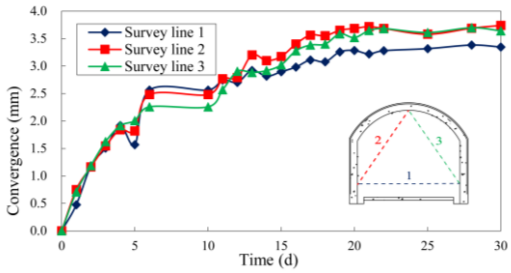

(a) convergence of 0+120 (construction tunnel ①)

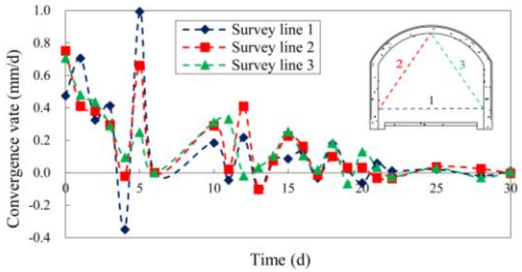

(b) convergence rate of 0+120 (construction tunnel ①)

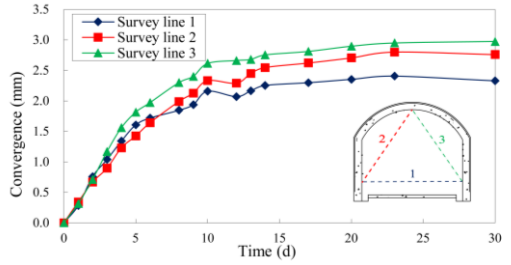

(c) convergence of 0+180 (construction tunnel ②)

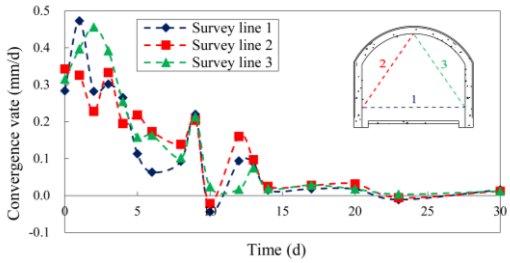

(d) convergence rate of 0+180 (construction tunnel ②)

Fig. 14 Convergence curve of each monitoring section after construction tunnel excavation

Table 5 Convergence of each monitoring section in construction tunnels

MS	S	MC (mm)	L (mm)	RDV (%)	T_1 (d)	MCR (mm/d)	T_2 (d)	OCR (mm/d)	TCC
0+120, ①	1	3.38	8845	0.038	28	1.00	6	0.11	Relatively stable
	2	3.74	7109	0.053	30	0.75	1	0.12	Relatively stable
	3	3.70	7430	0.050	28	0.71	1	0.12	Relatively stable
0+180, ②	1	2.40	8765	0.027	23	0.47	2	0.08	Stable
	2	2.80	7149	0.039	23	0.34	1	0.09	Stable
	3	2.98	7314	0.041	30	0.46	3	0.10	Stable

*MS: Monitoring section; S: Survey line; MC: Maximum convergence; L: Line length; RDV: Relative displacement value; T1: Time taken to reach maximum convergence; MCR: Maximum convergence rate; T2: Time between maximum convergence rate and start of monitoring; OCR: Overall convergence rate; TCC: Trend of convergence curve

14 days after tunnel excavation. Special sections require enhanced observation, such as the 1 + 570 and 1 + 630 sections of construction tunnel ②.

The surrounding rock convergence was monitored with a steel rule convergence meter, and the layout of the survey lines is shown on the right of each panel in Fig. 14. Survey line 1 was used to monitor the horizontal convergence, and survey lines 2 and 3 were used to monitor the vertical convergence. Within 24 h after excavation, measuring points were arranged on both sides and the crown arch of the tunnel. During observation, the convergence ruler was fixed between two measuring points, and a certain tension was applied to ensure that the convergence meter was in a tensioned state. Each time the length of the survey line was measured, the difference between the two was the convergence value of the survey line.

The measuring points on the left and right sides of section 0+120 (construction tunnel ①) are both 2.1 m away from the ground, and the measuring points on the left and right sides of section 0+180 (construction tunnel ②) are 2.0 m and 1.8 m away from the ground, respectively. Table 5 shows the surrounding rock convergence of each monitored section in the construction tunnel. According to the results, for the current surrounding rock and support conditions, the convergence characteristics of the construction tunnel are as follows:

1) The vertical convergence of the construction tunnel is greater than that of the horizontal convergence. The vertical convergence is approximately 0.4 mm larger than the horizontal convergence. The maximum convergence value is generally approximately 4 mm, and the ratio of that to the tunnel diameter (8.5 m) is not more than 0.05%, which meets the control standard.

2) It takes approximately 20-30 days for the surrounding rock convergence of the tunnel to stabilize, and sometimes even longer. The time required for the surrounding rock convergence to become stable is longer than that of crown settlement.

3) It can be seen from the contrast observation of survey lines 2 and 3 that the bias is not obvious.

4.2.2 Connection tunnel

Because the connection tunnel is directly connected to the storage cavern and there is an intersection with the

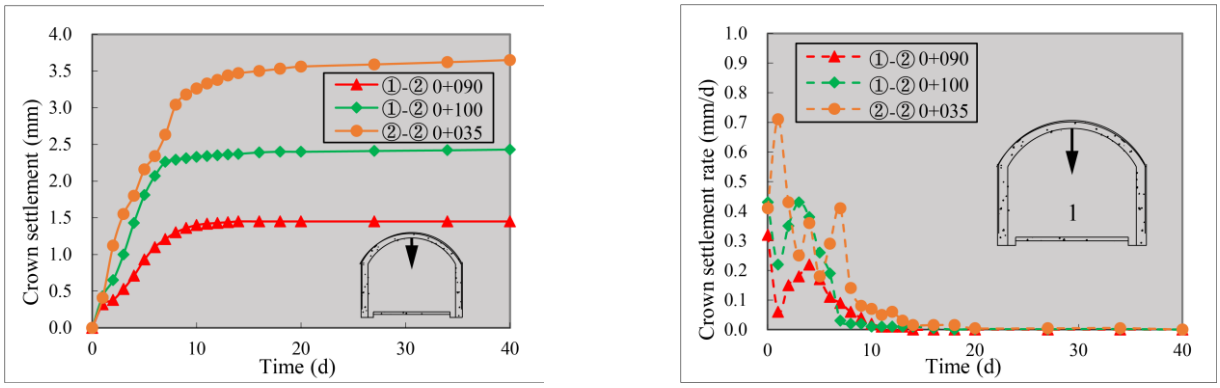

(a) crown settlement of construction tunnel ① (b) crown settlement rate of construction tunnel ②

Fig. 15 Crown settlement curve of connection tunnel after excavation

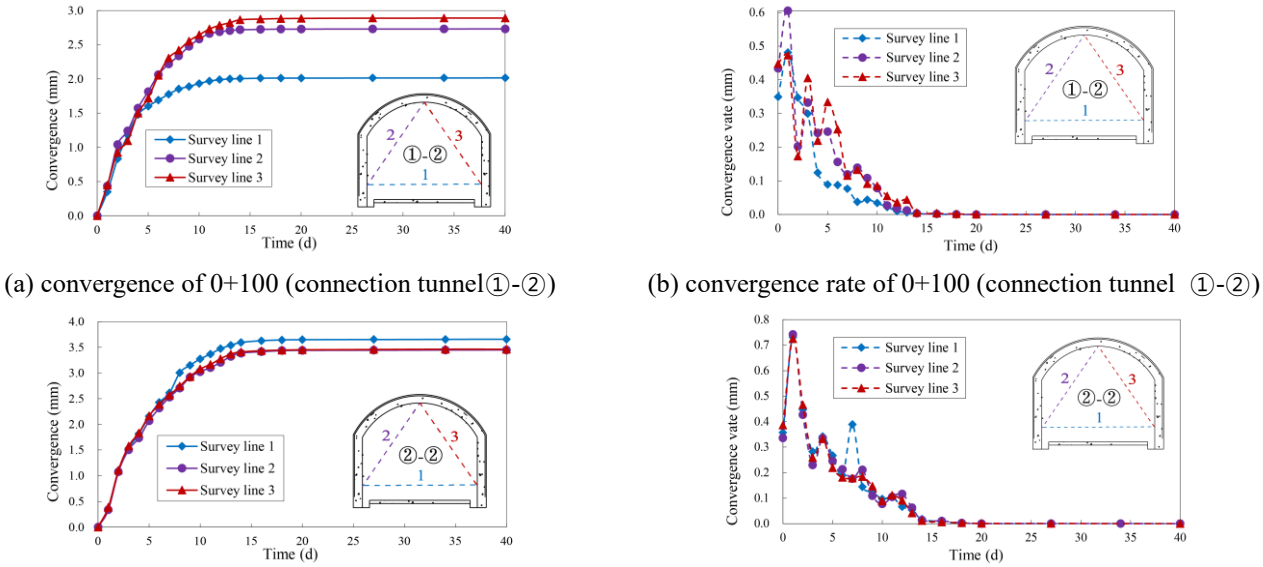

(a) convergence of 0+100 (connection tunnel①-②) (b) convergence rate of 0+100 (connection tunnel ①-②)

(c) convergence of 0+035 (connection tunnel ②-②) (d) convergence rate of 0+035 (connection tunnel ②-②)

Fig. 16 Convergence curve of connection tunnel after excavation

storage cavern, it is very important to monitor the displacement of the connection tunnel. The monitoring results of connection tunnels ①-② and ②-② were selected. Compared with the construction tunnel, the entire crown settlement of the connection tunnel is smaller. Among the three sets of data selected in Fig. 15, the crown settlement and settlement rate of connection tunnel ②-② are the largest. This indicates that the stability of the intersection of the connection tunnel and cavern #1 is worse than that of the intersection between the connection tunnel and cavern #3. For the current surrounding rock and support conditions, the crown settlement characteristics of the connection tunnel are:

1) At the intersection between the connection tunnel and the main cavern (shape "T"), the total crown settlement is 3.5 mm, which meets the control standard of the allowable relative displacement. The maximum crown settlement rate after excavation is approximately 0.7 mm/d. About 10 days after excavation, the settlement tends to be stable.

2) At the intersection between the connection tunnel and construction tunnel (shape "X"), the total crown settlement is 1.5-2.5 mm. The maximum crown settlement rate after excavation is approximately 0.45 mm/d. The time required for the surrounding rock to become stable is approximately seven days. It still meets the control standard of the allowable relative displacement.

The measuring points on the left and right sides of section 0+100 (connection tunnel ①-②) are both 2.0 m above the ground, and the measuring points on the left and right sides of section 0+035 (connection tunnel ②-②) are both 2.1 m above the ground (see Fig. 16). Overall, there is little difference between the convergence characteristics of the connection tunnel and construction tunnel. The horizontal convergence of connection tunnel ②-② is abnormally large. For the current surrounding rock and support conditions, the convergence characteristics of the connection tunnel are as follows:

1) At the intersection of the connection tunnel and the main cavern (shape "T"), the total convergence of the

surrounding rock is approximately 3.5 mm, which meets the requirements of allowable relative displacement. The initial convergence rate after excavation is approximately 0.73 mm/d. Approximately 15 days after excavation, convergence tends to be stable.

2) At the intersection of the connection tunnel and construction tunnel (shape "X"), the vertical convergence is approximately 3.0 mm, and the horizontal convergence is approximately 2.0 mm. The maximum convergence rate after excavation is approximately 0.5 mm/d, which still meets the requirements of allowable relative displacement.

5. Discussion

Based on the numerical simulation and field monitoring of the space-time evolution, this study reexamines the design and excavation aspects of underground water-sealed oil caverns. From the perspective of the whole cavern group rather than a single cavern, the influence of auxiliary tunnels is taken into account. The results show that the auxiliary tunnel has a non-negligible influence on the displacement field of storage caverns after excavation, especially at the intersection of the connection tunnels and the storage cavern. With respect to stability, we compare the difference in deformation characteristics of the surrounding rock in different design and excavation stages.

The site selection condition of water-sealed caverns is very strict. The right conditions for both stability and water-sealing ability must be satisfied. Compared with other underground engineering applications such as traffic tunnels and hydraulic tunnels, underground oil storage caverns have large sections with high sidewalls and large spans. Therefore, to ensure stability, it is necessary to select a stable, high-strength stratum as the reservoir area. The satisfaction of the water sealing requirement should be ensured in three respects: (1) selecting an area with sufficient groundwater and a stable water level as much as is possible; (2) in the construction stage, the loss of groundwater must be minimized, and during excavation the irreversible seepage of groundwater must be curtailed; (3) an artificial water curtain system is used to supply the underground water level during operation. A number of joint fissures distributed in the rock mass is an important channel for groundwater seepage, but it is also known that the fracture is unfavorable to the stability of the structure. Shotcrete contributes to the stability of the surrounding rock, but it also blocks the channels, which is not conducive to water sealing. Because groundwater level forms a groundwater depression cone over disturbed zones, it is reasonable to revisit the design and excavation principles that have a positive effect on the stability and water-sealing ability.

5.1 Design and excavation

With respect to cavern group design, design-A has the best stability performance when a construction tunnel is only connected to two caverns, which is also the reason why this design has been successfully adopted at the underground oil storage caverns located on the southeast coast of China (Shi *et al.* 2018). Design-B is changed into a cavern group of three caverns by extending the connection tunnel and connecting an additional cavern to the outside. The efficiency of this cavern group design is higher, but the stability is lower. Although it still meets the allowable relative displacement, the crown settlement of the middle cavern has been significantly increased by 24% (6.7 mm → 8.4 mm), which is not feasible in poor geological conditions. Design-B can be applied in practice by selecting the suitable support and the location of the connection tunnel in combination with geological conditions.

Long-term field monitoring shows that the auxiliary tunnels built in hard rock perform well in terms of stability. The two monitoring projects of crown settlement and surrounding rock convergence indicate that the stability can be satisfied under current geological conditions and support, which is also consistent with the numerical simulation results. The relation presented by the simulation and monitoring results is roughly the same. At the intersection between the connection tunnel and the construction tunnel, the settlement is smaller than that between the main caverns. At the intersection of the connection tunnel and the main caverns, the settlement of the middle cavern is significantly increased (Fig. 7(b)). Starting from the connection tunnel, the multi-step excavation method is adopted to carry out the excavation of three caverns synchronously, and the displacement changes of each feature point are different. During the excavation from the upper to the lower step, the displacement near the sidewall of the main cavern changes abnormally, which seems to show "first convergence and then divergence." However, the sidewall cannot move outward under the action of lateral stress. We believe that the displacement direction at the sidewall is not necessarily completely perpendicular to the sidewall, and part of the settlement displacement should also lead to the numerical change. The stability of the sidewalls will be further studied.

5.2 Spatial effect

After the excavation of large section caverns, there is a significant spatial effect in underground engineering. The rock mass in front of the tunnel face is deformed before excavation. Therefore, the displacement data obtained by conventional monitoring means represents the displacement after excavation. Through numerical calculations, we obtained the theoretical total displacement of the corresponding monitoring sections, which are shown in Tables 6 and 7. In the tables, monitoring values (daily monitoring values three months after excavation) and simulation values of crown settlement are given, and three evaluation indices are introduced: the ratio of monitoring values to simulation values (R), settlement difference (S), and percentage of settlement difference to tunnel diameter (8.5 m or 20 m) (P). The first (R) is the ratio of the settlement amount after excavation to the total settlement amount, the second (S) represents the settlement portion not recorded by monitoring, and the third (P) represents the percentage displacement of S relative to the tunnel

Table 6 Comparison between the monitoring and simulation values of the crown settlement-connection tunnel

N	Chainage	Crown settlement		R	S (mm)	P (8.5 m)
		Monitoring value (value after excavation) (mm)	simulation value (total value) (mm)			
1-1	0+065	3.62	7.41	0.49	3.79	0.045%
	0+080	3.27	5.42	0.60	2.15	0.025%
	0+135	3.71	6.02	0.62	2.31	0.027%
1-2	0+035	3.65	6.34	0.58	2.69	0.032%
	0+90	1.47	5.72	0.26	4.25	0.050%
	0+100	2.43	6.45	0.38	4.02	0.047%
1-3	0+130	1.79	3.08	0.58	1.29	0.015%

*N: Number of connection tunnel; R: the ratio of monitoring values to simulation values; S: settlement difference; P: percentage of settlement difference to tunnel diameter

Table 7 Comparison between the monitoring and simulation values of the crown settlement-storage cavern

N	Chainage	Crown settlement		R	S (mm)	P (20 m)
		Monitoring value (value after excavation) (mm)	simulation value (total value) (mm)			
#1	0 + 245	7.07	6.89	1.03	−0.18	−0.001%
	0 + 360	4.51	7.74	0.58	3.23	0.016%
	0 + 420	4.42	7.2	0.61	2.78	0.014%
#2	0 + 370	4.17	8.54	0.49	4.37	0.022%
	0 + 428	3.77	7.79	0.48	4.02	0.020%
	0 + 360	4.02	7.01	0.57	2.99	0.015%
#3	0 + 420	3.98	6.69	0.59	2.71	0.014%
	0 + 470	3.30	6.22	0.53	2.92	0.015%

*N: Number of storage caverns; R: the ratio of monitoring values to simulation values; S: settlement difference; P: percentage of settlement difference to tunnel diameter

diameter. It should be noted that since the model does not consider the influence of support, the simulation value is the total displacement of no support. There is a support system in practice, and the total displacement under the support condition includes the displacement value before excavation and the displacement value after excavation, of which the monitoring value is the latter (the monitoring instrument is buried after excavation).

In Table 6, the crown settlements of connection tunnels in group 1 are compared. The crown settlement after excavation accounts for about 50-60% of the total settlement. The indices S and P are all within the allowable range of the standard. However, at 0+065 of 1-1, and 0+90 and 0+100 of connection tunnel 1-2, the indices S and P are large, indicating that a large part of the settlement will have been carried out before the operation of the monitoring instrument. The possible reasons are as follows: (a) there is a fracture zone with poor stability, (b) the surrounding rock produced a significant amount of displacement after excavation due to the untimely support, and (c) the operation monitoring instrument was not installed within the allowed time limit. In Table 7, the crown settlements of the three main caverns in group 1 are compared, and the crown settlement after excavation accounts for about 50-60% of the total settlement, which is the same as that of the connection tunnel. Because the cavern section is larger, the index S is generally larger, and the index P is smaller, but all of them are within the allowable range of the standard. The settlement monitoring value of cavern #1 is 7.07 mm, which exceeds the total displacement value calculated. The possible reason for this is that the stability of the surrounding rock in this area is poor, and the support needs to be strengthened. Special attention should be paid to strengthen the observation. For hard rock tunnel construction, it is generally recognized that the deformation in front of the tunnel face (the displacement value before excavation) under normal surrounding rock conditions is about 20-30% of the total deformation, and the deformation value after excavation is about 60-70% of the total deformation. Because the model does not consider the support, the deformation simulation value is slightly large, so the R (50-60%) is generally small.

The supporting behavior is positive to the construction, and the immediate supporting after excavation is helpful to control surrounding rock deformation. By comparing the crown settlements before and after excavation, the displacement space characteristics of underground caverns after excavation are mastered. The higher the quality and strength of the surrounding rock, the lower the displacement before and after excavation, and the lower the proportion of settlement before excavation. However, in areas with poor stability, the total crown settlement and the proportion of

settlement before excavation may increase correspondingly. This study also reflects the importance of pre-grouting reinforcement measures, timely support, and installation of monitoring instruments after excavation.

6. Conclusion

Based on a comprehensive analysis of numerical calculations and field monitoring, the design and excavation stability of underground water-sealed oil storage caverns were studied, with the cavern group, including storage caverns and auxiliary tunnels, as the subject. In addition, we compared the displacement before and after the excavation. The results show that among the intersection of the connection tunnel and other tunnels, the stability of the intersection at the main cavern is the weakest. Comparing the two types of cavern group designs, the settlement difference at the intersection of the middle cavern and the connection tunnel is the largest. It is feasible to expand from the two-cavern group to the three-cavern group. The displacement characteristics of different feature points in a section have large differences in different construction steps. In particular, when different steps are excavated, the convergence space-time evolution of different feature points in the section is different. The crown arch of the main cavern is the least stable in the entire area of the cavern group, while the stability of the connection tunnel is better. The relative value of the surrounding rock displacement after excavation in the research meets the control standards. The final relative displacement of the tunnel section does not exceed 4 mm, the initial maximum convergence rate is 0.5-0.8 mm/d, the crown settlement tends to be stable after excavation for 10-14 days, and the convergence takes about 30 days to stop. The crown settlement after excavation accounts for approximately 50%–60% of the total settlement. We hope that this study could help in the future designing of underground oil cavern groups and auxiliary tunnel layouts and provide theoretical support for the formation pretreatment, optimization of excavation steps and monitoring scheme, and layering and strengthening support.

Acknowledgments

The research described in this paper was financially supported by the National Natural Science Foundation of China (grant numbers 41877239, 51379112, 51422904, 40902084 and 41772298), and Fundamental Research Funds for the Central Universities (grant number 2018JC044), and Natural Science Foundation of Shandong Province (grant number JQ201513).

References

Aberg, B. (1977), "Prevention of gas leakage from unlined reservoir in rock", *Proceedings of 1st International Symposium on Storage in Excavated Rock Caverns*, Stockholm, September.

Aliyu, M.M., Shang, J., Murphy, W., Lawrence, J.A., Collier, R., Kong, F. and Zhao, Z. (2019), "Assessing the uniaxial compressive strength of extremely hard cryptocrystalline flint", *Int. J. Rock Mech. Min.*, **113**, 310-321.https://doi.org/10.1016/j.ijrmms.2018.12.002.

Benardos, A.G. and Kaliampakos, D.C. (2005), "Hydrocarbon storage in unlined rock caverns in greek limestone", *Tunn. Undergr. Sp. Tech.*, **20**, 175-182.https://doi.org/10.1016/j.tust.2004.08.005.

Chen, Y. and Irfan, M. (2018), "Experimental study of kaiser effect under cyclic compression and tension tests", *Geomech. Eng.*, **14**, 203-209.https://doi.org/10.12989/gae.2018.14.2.203.

Daraei, A. and Zare, S. (2018), "A new strain-based criterion for evaluating tunnel stability", *Geomech. Eng.*, **16**(2), 205-215. http://dx.doi.org/10.12989/gae.2018.16.2.205.

Deng, J.Q., Yang, Q., Liu, Y.R. and Pan, Y.W. (2015), "Stability evaluation and failure analysis of rock salt gas storage caverns based on deformation reinforcement theory", *Comput. Geotech.*, **68**, 147-160.https://doi.org/10.1016/j.compgeo.2015.03.013.

Goodall, D.C., Aberg, B. and Brekke, T.L. (1988), "Fundamentals of gas containment in unlined rock caverns", *Rock Mech. Rock Eng.*, **21**, 235-258.https://doi.org/10.1007/Bf01020278.

He, L. and Zhang, Q.B. (2015), "Numerical investigation of arching mechanism to underground excavation in jointed rock mass", *Tunn. Undergr. Sp. Tech.*, **50**, 54-67. https://doi.org/10.1016/j.tust.2015.06.007.

Hong, J.S., Lee, H.S., Lee, D., Kim, H., Choi, Y.T. and Park, Y. (2006), "Microseismic event monitoring of highly stressed rock mass around underground oil storage caverns", *Tunn. Undergr. Sp. Tech.*, **21**, 292.

Hoshino, K. (1993), "Construction of underground caverns for petroleum storage in orogenic areas - geological stability", *Eng. Geol.*, **35**, 199-205. https://doi.org/10.1016/0013-7952(93)90007-Y.

Kong, F. and Shang, J. (2018), "A validation study for the estimation of uniaxial compressive strength based on index tests", *Rock Mech. Rock Eng.*, **51**, 2289-2297. https://doi.org/10.1007/s00603-018-1462-9.

Lee, C.I. and Song, J.J. (2003), "Rock engineering in underground energy storage in korea", *Tunn. Undergr. Sp. Tech.*, **18**, 467-483.https://doi.org/10.1016/S0886-7798(03)00046-4.

Li, S.C., Wang, J.H., Chen, W.Z., Li, L.P., Zhang, Q.Q. and He, P. (2016), "Study on mechanism of macro failure and micro fracture of local nearly horizontal stratum in super-large section and deep buried tunnel", *Geomech. Eng.*, **11**(2), 253-267. http://dx.doi.org/10.12989/gae.2016.11.2.253.

Li, S.C., Wang, Z.C., Ping, Y., Zhou, Y. and Zhang, L. (2014), "Discrete element analysis of hydro-mechanical behavior of a pilot underground crude oil storage facility in granite in China", *Tunn. Undergr. Sp. Tech.*, **40**, 75-84. https://doi.org/10.1016/j.tust.2013.09.010.

Li, Z., Xue, Y., Liang, J., Qiu, D., Su, M. and Kong, F. (2020), "Performance assessment of the water curtain system: A monitoring system in an underground water-sealed oil reservoir in China", *B. Eng. Geol. Environ*., https://doi.org/10.1007/s10064-020-01792-0.

Li, Z.Q., Xue, Y.G., Li, S.C., Qiu, D.H., Su, M.X., Zhao, Y. and Zhou, B.H. (2019), "An analytical model for surrounding rock classification during underground water-sealed caverns construction: A case study from eastern China", *Environ. Earth. Sci.*, **78**(20), 1-11. https://doi.org/10.1007/s12665-019-8606-4.

Liu, J., Zhao, X.D., Zhang, S.J. and Xie, L.K. (2018), "Analysis of support requirements for underground water-sealed oil storage cavern in China", *Tunn. Undergr. Sp. Tech.*, **71**, 36-46. https://doi.org/10.1016/j.tust.2017.08.013.

Ma, K., Tang, C.A., Wang, L.X., Tang, D.H., Zhuang, D.Y., Zhang, Q.B. and Zhao, J. (2016), "Stability analysis of underground oil storage caverns by an integrated numerical and

microseismic monitoring approach", *Tunn. Undergr. Sp. Tech.*, **54**, 81-91. https://doi.org/10.1016/j.tust.2016.01.024.

Ma, X.D. and Haimson, B.C. (2016), "Failure characteristics of two porous sandstones subjected to true triaxial stresses", *J. Geophys. Res.-Sol. Ea.*, **121**, 6477-6498.https://doi.org/10.1002/2016jb012979.

Ma, X.D. and Zoback, M.D. (2017), "Laboratory experiments simulating poroelastic stress changes associated with depletion and injection in low-porosity sedimentary rocks", *J. Geophys. Res.-Sol. Ea.*, **122**, 2478-2503.https://doi.org/10.1002/2016jb013668.

Mawire, A. (2013), "Experimental and simulated thermal stratification evaluation of an oil storage tank subjected to heat losses during charging", *Appl. Energ.*, **108**, 459-465.https://doi.org/10.1016/j.apenergy.2013.03.061.

Mohanty, S. and Vandergrift, T. (2012), "Long term stability evaluation of an old underground gas storage cavern using unique numerical methods", *Tunn. Undergr. Sp. Tech.*, **30**, 145-154.https://doi.org/10.1016/j.tust.2012.02.015.

Nawel, B. and Salah, M. (2015), "Numerical modeling of two parallel tunnels interaction using three-dimensional Finite Elements Method", *Geomech. Eng.*, **9**(6), 775-791. http://dx.doi.org/10.12989/gae.2015.9.6.775.

Ning, Z., Xue, Y., Su, M., Qiu, D., Zhang, K., Li, Z. and Liu, Y. (2021), "Deformation characteristics observed during multi-step excavation of underground oil storage caverns based on field monitoring and numerical simulation", *Environ. Earth. Sci.,* **80**, 222.https://doi.org/10.1007/s12665-021-09496-8.

Oh, J., Moon, T., Canbulat, I. and Moon, J.S. (2019), "Design of initial support required for excavation of underground cavern and shaft from numerical analysis", *Geomech. Eng.*, **17**, 573-581.https://doi.org/10.12989/gae.2019.17.6.573.

Qiao, L.P., Li, S.C., Wang, Z.C., Tian, H. and Bi, L.P. (2016), "Geotechnical monitoring on the stability of a pilot underground crude-oil storage facility during the construction phase in china", *Meas.*, **82**, 421-431.https://doi.org/10.1016/j.measurement.2016.01.017.

Shang, J., Hencher, S.R., West, L.J. and Handley, K. (2017), "Forensic excavation of rock masses: A technique to investigate discontinuity persistence", *Rock Mech. Rock Eng.*, **50**, 2911-2928.https://doi.org/10.1007/s00603-017-1290-3.

Shi, L., Zhang, B., Wang, L., Wang, H.X. and Zhang, H.J. (2018), "Functional efficiency assessment of the water curtain system in an underground water-sealed oil storage cavern based on time-series monitoring data", *Eng. Geol.*, **239**, 79-95. https://doi.org/10.1016/j.enggeo.2018.03.015.

Sturk, R. and Stille, H. (1995), "Design and excavation of rock caverns for fuel storage—a case study from zimbabwe", *Tunn. Undergr. Sp. Tech.*, **10**, 193-201. https://doi.org/10.1016/0886-7798(95)00007-l.

Tal, Y., Hatzor, Y.H. and Feng, X.T. (2014), "An improved numerical manifold method for simulation of sequential excavation in fractured rocks", *Int. J. Rock Mech. Min.*, Sciences **65**, 116-128. https://doi.org/10.1016/j.ijrmms.2013.10.005.

Wang, Z., Glais, Y., Qiao, L., Huang, A. and Liu, J. (2018), "Hydro-geochemical analysis of the interplay between the groundwater, host rock and water curtain system for an underground oil storage facility", *Tunn. Undergr. Sp. Tech.*, **71**, 466-477. https://doi.org/10.1016/j.tust.2017.10.001.

Wang, Z.C., Kwon, S., Qiao, L.P., Bi, L.P. and Yu, L.Y. (2017), "Estimation of groundwater inflow into an underground oil storage facility in granite", *Geomech. Eng.,* **12**(7), 1003-1020.http://dx.doi.org/10.12989/gae.2017.12.6.1003.

Wang, Z.C., Li, S.C. and Qiao, L.P. (2015), "Design and test aspects of a water curtain system for underground oil storage caverns in China", *Tunn. Undergr. Sp. Tech.*, **48**, 20-34. https://doi.org/10.1016/j.tust.2015.01.009.

Xue, Y.G., Li, S.C., Qiu, D.H., Wang, Z.C., Li, Z.Q., Tian, H., Su, M.X., Yang, W.M., Lin, C.J. and Zhu, J.Y. (2015), "A new evaluation method for site selection of large underground water-sealed petroleum storage depots", *Sci. China-Technol. Sc.*, **58**, 967-978. https://doi.org/10.1007/s11431-015-5825-0.

Xue, Y.G., Ning, Z.X., Qiu, D.H., Su, M.X., Li, Z.Q., Kong, F.M., Li, G.K. and Wang, P. (2021), "A study of water curtain parameters of underground oil storage caverns using time series monitoring and numerical simulation", *J. Zhejiang. Univ. Sci. A.,* **22**(3), 165-181. https://doi.org/10.1631/jzus.A 2000130.

Yang, T.H., Jia, P., Shi, W.H., Wang, P., Liu, H.L. and Yu, Q.L. (2014), "Seepage-stress coupled analysis on anisotropic characteristics of the fractured rock mass around roadway", *Tunn. Undergr. Sp. Tech.*, **43**, 11-19. https://doi.org/10.1016/j.tust.2014.03.005.

Yoo, C. (2016), "Effect of spatial characteristics of a weak zone on tunnel deformation behavior", *Geomech. Eng.*, **11**(1), 41-58. http://dx.doi.org/10.12989/gae.2016.11.1.041.

Yoo, C. and Choi, J. (2018), "Effect of construction sequence on three-arch tunnel behavior-Numerical investigation", *Geomech. Eng.*, **15**(3), 911-917. http://dx.doi.org/10.12989/gae.2018.15.3.911.

Zhang, B., Shi, L., Yu, X. and Qi, S.W. (2019), "Assessing the water-sealed safety of an operating underground crude oil storage adjacent to a new similar cavern - A case study in china", *Eng. Geol.*, **249**, 257-272.https://doi.org/10.1016/j.enggeo.2019.01.008.

Zhu, W.S., Li, X.J., Zhang, Q.B., Zheng, W.H., Xin, X.L., Sun, A.H. and Li, S.C. (2010), "A study on sidewall displacement prediction and stability evaluations for large underground power station caverns", *Int. J. Rock Mech. Min.*, **47**, 1055-1062.https://doi.org/10.1016/j.ijrmms.2010.07.008.

Zhuang, D.Y., Tang, C.A., Liang, Z.Z., Ma, K., Wang, S.Y. and Liang, J.Z. (2017), "Effects of excavation unloading on the energy-release patterns and stability of underground water-sealed oil storage caverns", *Tunn. Undergr. Sp. Tech.*, **61**, 122-133. https://doi.org/10.1016/j.tust.2016.09.011.

GC